KRAS4A induces metastatic lung adenocarcinomas in vivo in the absence of the KRAS4B isoform

Marina Salmón[a,1], Guillem Paniagua[a,1], Carmen G. Lechuga[a], Fernando Fernández-García[a], Eduardo Zarzuela[b,c], Ruth Álvarez-Díaz[a], Monica Musteanu[a,d], Carmen Guerra[a], Eduardo Caleiras[e], Javier Muñoz[b,c], Sagrario Ortega[f], Matthias Drosten[a,2,3], and Mariano Barbacid[a,2,3]

[a]Experimental Oncology, Molecular Oncology Programme, Centro Nacional de Investigaciones Oncológicas, 28029 Madrid, Spain; [b]Proteomics Unit, Biotechnology Programme, Centro Nacional de Investigaciones Oncológicas, 28029 Madrid, Spain; [c]ProteoRed, Instituto de Salud Carlos III, 28049 Madrid, Spain; [d]Department of Biochemistry and Molecular Biology, Faculty of Pharmacy, Complutense University, 28040 Madrid, Spain; [e]Histopathology Unit, Biotechnology Programme, Centro Nacional de Investigaciones Oncológicas, 28029 Madrid, Spain; and [f]Mouse Genome Editing Unit, Biotechnology Programme, Centro Nacional de Investigaciones Oncológicas, 28029 Madrid, Spain

Contributed by Mariano Barbacid, June 15, 2021 (sent for review November 5, 2020; reviewed by Frank McCormick and Mark R. Philips)

In mammals, the *KRAS* locus encodes two protein isoforms, KRAS4A and KRAS4B, which differ only in their C terminus via alternative splicing of distinct fourth exons. Previous studies have shown that whereas KRAS expression is essential for mouse development, the KRAS4A isoform is expendable. Here, we have generated a mouse strain that carries a terminator codon in exon 4B that leads to the expression of an unstable KRAS4B^{154} truncated polypeptide, hence resulting in a bona fide *Kras*4B-null allele. In contrast, this terminator codon leaves expression of the KRAS4A isoform unaffected. Mice selectively lacking KRAS4B expression developed to term but died perinatally because of hypertrabeculation of the ventricular wall, a defect reminiscent of that observed in embryos lacking the *Kras* locus. Mouse embryonic fibroblasts (MEFs) obtained from *Kras*4B$^{-/-}$ embryos proliferated less than did wild-type MEFs, because of limited expression of KRAS4A, a defect that can be compensated for by ectopic expression of this isoform. Introduction of the same terminator codon into a *Kras*^{FSFG12V} allele allowed expression of an endogenous KRAS4A^{G12V} oncogenic isoform in the absence of KRAS4B. Exposure of *Kras*$^{+/FSF4AG12V4B-}$ mice to Adeno-FLPo particles induced lung tumors with complete penetrance, albeit with increased latencies as compared with control *Kras*$^{+/FSFG12V}$ animals. Moreover, a significant percentage of these mice developed proximal metastasis, a feature seldom observed in mice expressing both mutant isoforms. These results illustrate that expression of the KRAS4A^{G12V} mutant isoform is sufficient to induce lung tumors, thus suggesting that selective targeting of the KRAS4B^{G12V} oncoprotein may not have significant therapeutic consequences.

KRAS isoforms | alternative splicing | gene editing | lung tumors | hypertrabeculation

The *KRAS* locus has gained prominence due to its involvement in as many as one-fourth of all human tumors (1, 2). This locus encodes two protein isoforms, KRAS4A and KRAS4B, via alternative splicing of independent fourth exons. Both proteins share almost identical amino acids from residues 1 to 164, a region that includes the guanosine triphosphate–binding domain, as well as the switch I and II regions responsible for engaging with their main downstream effectors (3–5). These residues also include all known oncogenic mutations. However, these isoforms differ substantially from residue 165 onward, a region that includes the hypervariable region (HVR) primarily involved in protein trafficking as well as in establishing its location within the plasma membrane (5, 6). Finally, both isoforms are prenylated at the cysteine residue of their respective CAAX boxes located at their C termini.

The KRAS4B protein contains a unique polybasic stretch not found in other RAS proteins formed by a series of lysine residues that presumably organizes its localization to distinct nanoclusters. In addition, KRAS4B can be phosphorylated at serine 181 within the polybasic stretch, which is believed to reduce the net charge of the HVR, thus decreasing its affinity for the plasma membrane (4). Binding of calmodulin to KRAS4B is known to block this phosphorylation step, although the functional significance remains a matter of debate (7, 8). Interestingly, calmodulin binding to oncogenic KRAS4B suppressed noncanonical Wnt signaling. Disruption of this interaction has been proposed to reduce the tumorigenic properties of mutant KRAS4B in pancreatic cancer (9). KRAS4A on the other hand uses a hybrid membrane-targeting motif consisting of an acylatable cysteine residue as well as a bipartite polybasic region and resides in disorganized liquid domains (10, 11). Moreover, lysine fatty acylation selectively regulates membrane distribution and in vitro transforming properties of KRAS4A (12). The distinct membrane distribution properties of KRAS4A have also been attributed to its association with HK1 in the outer mitochondrial membrane, an activity that is not shared by KRAS4B (13).

Despite these differences in their HVR, the biological significance of the two KRAS isoforms is less clear. Whereas genetic

Significance

KRAS encodes two protein isoforms which differ in intracellular trafficking and plasma membrane location. Moreover, *KRAS* mutations in cancer activate both isoforms. Thus, understanding their individual contributions to tumor development may facilitate the design of therapeutic strategies to selectively target each isoform. Here, we describe two strains of mice that fail to express KRAS4B without affecting expression of either wild-type KRAS4A or oncogenic KRAS4A^{G12V}. Expression of KRAS4A in the absence of KRAS4B prevents postnatal development. More importantly, expression of the endogenous KRAS4A^{G12V} isoform in the absence of KRAS4B is sufficient to induce lung adenocarcinomas that undergo proximal metastasis. Hence, development of therapeutic strategies against KRAS mutant tumors must take into account inhibition of both protein isoforms.

Author contributions: S.O., M.D., and M.B. designed research; M.S., G.P., C.G.L., F.F.-G., E.Z., R.A.-D., J.M., and M.D. performed research; E.C. provided histopathological advice; S.O. provided gene-editing advice; M.M. and C.G. contributed critical information and helpful discussions; M.S., G.P., F.F.-G., E.Z., R.A.-D., M.M., C.G., J.M., S.O., M.D., and M.B. analyzed data; and M.D. and M.B. wrote the paper.

Reviewers: F.M., University of California, San Francisco; and M.R.P., New York University School of Medicine.

The authors declare no competing interest.

[1]M.S. and G.P. contributed equally to this work.

[2]M.D. and M.B. contributed equally to this work.

[3]To whom correspondence may be addressed. Email: mdrosten@cnio.es or mbarbacid@cnio.es.

This article contains supporting information online at https://www.pnas.org/lookup/suppl/doi:10.1073/pnas.2023112118/-/DCSupplemental.

Published July 22, 2021.

disruption of the entire *Kras* locus causes embryonic lethality at midgestation, selective ablation of the KRAS4A isoform did not result in any obvious phenotype either during embryonic development or adult homeostasis, thus suggesting that expression of KRAS4B is sufficient to perform most of the KRAS functions in mice (14–16). Indeed, KRAS4B appears to represent the majority of the two isoforms during embryonic development, while KRAS4A is more dynamically regulated and its ratio slightly increases in several adult tissues (17). Several studies, however, have detected widespread expression of KRAS4A in *RAS* mutant cancers (10, 18, 19). In addition, absence of KRAS4A reduced tumorigenesis when using a chemical carcinogenesis model of lung cancer (20). Finally, knockin of a KRAS4B complementary DNA (cDNA) into the *Kras* locus following a strategy that eliminates KRAS4A expression rendered mice largely resistant to chemical carcinogenesis (21).

To better understand the unique role(s) of the KRAS4A isoform in normal and tumor-bearing mice, we have generated wild-type and oncogenic *Kras* alleles that prevent expression of the KRAS4B isoform without altering the overall genomic structure of the *Kras* locus, hence not affecting expression of either wild-type or mutant KRAS4A isoforms, respectively. These studies provide important insights into the role of the KRAS4A isoform both during embryonic development and in tumor formation.

Results

Generation of KRAS4B-Deficient Mice. To genetically interrogate the requirement for KRAS4B in normal homeostasis as well as in tumor development, we generated a mouse strain in which expression of the KRAS4B isoform was selectively eliminated without affecting expression of KRAS4A (Fig. 1*A*). To this end, we introduced a TGA stop codon within positions 13 to 15 of *Kras* exon 4B by microinjecting a single-stranded DNA oligonucleotide as a template for homologous recombination together with a single-guide RNA (sgRNA) and the recombinant Cas9 protein into mouse embryos (Fig. 1*B*). The position of the stop codon was chosen to eliminate the protospacer adjacent motif (PAM) (AGG) to prevent recleavage of the DNA after homologous recombination (Fig. 1*B*). For screening purposes, we also introduced another point mutation at position 21 in exon 4B to generate a diagnostic XbaI restriction site (Fig. 1*B*). The TGA stop codon replaces codon 155 (GCC, Ala), resulting in the generation of a truncated KRAS4B protein (KRAS4B^{154}) that lacks the 34 carboxyl-terminal amino acids that include most of the α5-helix and the entire polybasic region as well as the CAAX domain (Fig. 1 *C* and *D*). This strategy predicts, as illustrated below, that the KRAS4B polypeptide expressed by the targeted allele will be unstable, representing a true "null" allele. Equally important, this targeting strategy preserves exon 4B including the large 3′ untranslated region (UTR) which is also present in the *Kras*4A transcript, thus preventing any potential deleterious effects on the expression of the KRAS4A isoform. Mice carrying the desired homologous recombination event were identified by XbaI digestion (*SI Appendix*, Fig. S1 *A* and *B*) followed by sequencing the genomic region spanning the homologous recombination event (*SI Appendix*, Fig. S1*C*). These mice were mated to wild-type mice of mixed 129/Sv-C57BL/6 background to confirm germline transmission. The resulting heterozygous mice were designated *Kras*4B$^{+/-}$ to indicate that the targeted *Kras* allele failed to express a functional KRAS4B isoform.

The KRAS4B Isoform Is Essential for Embryonic Development. Heterozygous *Kras*4B$^{+/-}$ mice were crossed among themselves to interrogate the requirements for KRAS4B expression during mouse development. Embryonic day 13.5 (E13.5) *Kras*4B$^{-/-}$ embryos were obtained slightly below the expected Mendelian ratios (20.8%) (*SI Appendix*, Table S1). Yet, they were indistinguishable from their wild-type littermates, not presenting any obvious defects. Similar

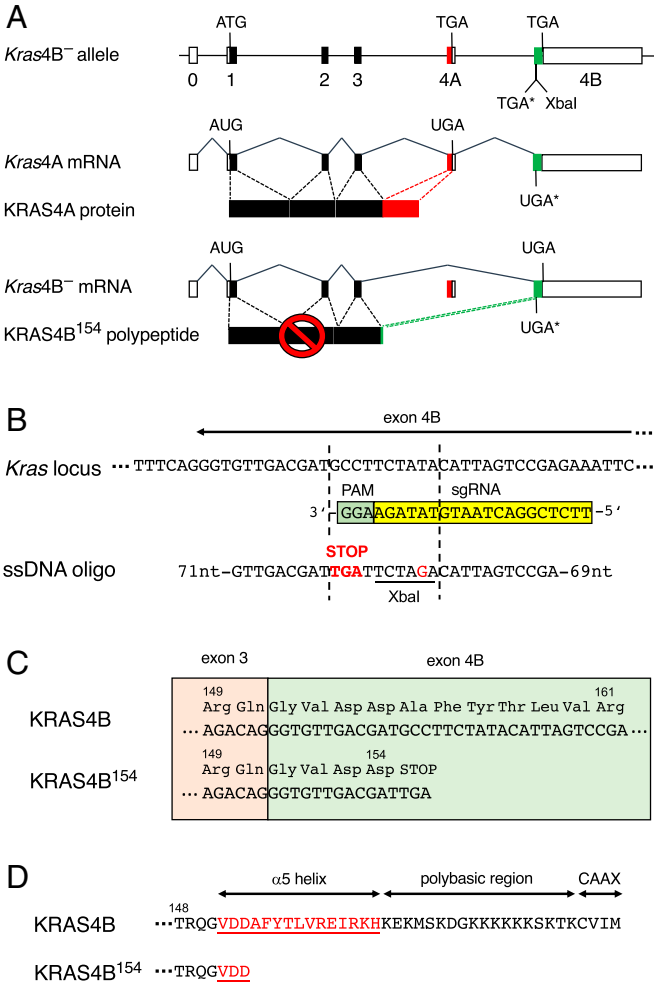

Fig. 1. Generation of mice lacking KRAS4B expression. (*A*) Schematic diagram depicting the generation of the *Kras*4B^{-} allele. (*A*, *Top*) Genomic structure of the *Kras*4B^{-} allele. Exons are indicated by numbered boxes. Noncoding sequences are represented by open boxes. Common coding sequences are shown as solid boxes. The coding sequences of exon 4A (red box) and exon 4B (green box) as well as the location of their respective stop codons (TGA) are also indicated. The engineered stop codon (TGA*) and the diagnostic XbaI restriction site are shown below the genomic structure. (*A*, *Middle*) mRNA transcripts and protein translation of the KRAS4A isoform. (*A*, *Bottom*) mRNA transcripts and translation of the truncated KRAS4B^{154} polypeptide. This polypeptide contains only four amino acid residues encoded by exon 4B sequences (in green). The location of the targeted terminator codon (UGA*) is indicated below the genomic structure. The "forbidden" sign on top of the KRAS4B^{154} protein indicates that this truncated protein is unstable and cannot be detected (see below). (*B*) Schematic representation of the CRISPR-Cas9 strategy used to target the exon 4B sequences. (*B*, *Top*) Wild-type 4B sequences corresponding to the targeted region. (*B*, *Middle*) sgRNA sequences are indicated by a yellow box. The adjacent PAM motif (green box) corresponds to the reverse strand. (*B*, *Bottom*) Targeted sequences indicating the knocked-in stop codon (STOP) and the point mutation needed to create an XbaI site are indicated in red. (*C*) DNA and triple-letter amino acid sequence of a fraction of the wild-type (*Top*) and recombinant (*Bottom*) KRAS4B cDNA. Sequences corresponding to exon 3 are enclosed in an orange box. Sequences corresponding to exon 4B are shown within a green box. (*D*) Single-letter amino acid sequences of KRAS4B (residues 149 to 188) and KRAS4B^{154} (residues 149 to 154). Residues corresponding to the α5-helix are indicated in red. Those residues corresponding to the polybasic domain and the CAAX motif present in the KRAS4B protein are also indicated.

ratios were observed at late embryonic development (E18.5, 19.7%), although 2 out of 16 embryos were already dead. E18.5 *Kras*4B$^{-/-}$embryos were smaller than their wild-type littermates and displayed heart abnormalities highly reminiscent of those detected in *Kras*-null embryos (Fig. 2*A*), although in the latter case embryos failed to progress starting from E12.5, with very few of them reaching E18.5 (15). Indeed, *Kras*4B$^{-/-}$ embryos exhibited a dramatic hypertrabeculation of the ventricular wall suggestive of defective myocardial compaction. Close examination of other tissues at E18.5 did not reveal significant histopathological abnormalities or alterations in proliferation or apoptosis, as determined by immunohistochemical analysis of Ki67 or cleaved caspase 3, respectively (*SI Appendix*, Fig. S2). However, we identified an increase in the common lymphoid progenitor population, indicating that fetal hematopoiesis is altered in *Kras*4B$^{-/-}$ embryos (Fig. 2*B* and *SI Appendix*, Fig. S3).

A limited proportion of *Kras*4B$^{-/-}$ embryos developed to term (6 out of 61 mice, 9.8%) (*SI Appendix*, Table S1). Yet, two of them were found dead immediately after birth and another three died within the first 6 to 8 h postpartum. Finally, we did not observe any *Kras*4B$^{-/-}$ mouse at postnatal day 21 (P21). In summary, these observations indicate that the KRAS4A isoform is sufficient to allow proper embryonic development of most mouse tissues but cannot compensate for the lack of KRAS4B expression during prenatal heart development.

The Truncated KRAS4B^{154} Protein Is Unstable. Cultures of primary mouse embryonic fibroblasts (MEFs) were generated from E13.5 wild-type and *Kras*4B$^{-/-}$ littermate embryos to define the unique contributions of KRAS4A and KRAS4B to cell proliferation. As expected, introduction of the stop codon in exon 4B did not change the levels of *Kras*4A messenger RNA (mRNA) expression (Fig. 3*A*). We also observed a 40% increase in the total levels of *Kras* mRNA in *Kras*4B$^{-/-}$ MEFs, as determined by qRT-PCR. This increase was exclusively due to an increase in the levels of the targeted *Kras*4B mRNA.

To determine the relative amounts of the two KRAS isoforms in these MEFs, we submitted cell extracts to Western blot analysis using a Pan KRAS antibody selective for both KRAS isoforms or a Pan RAS antibody that detects all RAS proteins. As expected, *Kras*4B$^{-/-}$ MEFs did not display detectable levels of KRAS proteins (Fig. 3*B*). In contrast, the expression levels of either HRAS or NRAS proteins were similar in wild-type and *Kras*4B$^{-/-}$ MEFs. In order to increase the sensitivity of detection, we incubated cell extracts with Pan RAS antibodies to immunoprecipitate all RAS proteins followed by Western blot analysis using either Pan KRAS or KRAS4A-specific antibodies (Fig. 3*B*). Under these conditions, we were able to detect the KRAS4A isoform in *Kras*4B$^{-/-}$ MEFs. However, neither technique revealed any expression of the truncated KRAS4B^{154} protein (Fig. 3*B*). As controls, both KRAS4B and KRAS4A isoforms were readily detected in RASless cells ectopically expressing these proteins (Fig. 3*B*).

To confirm that these results were indeed due to the instability of the truncated KRAS4B^{154} protein, we generated cDNAs encoding fusion proteins between wild-type KRAS4B or truncated KRAS4B^{154} with enhanced green fluorescent protein (EGFP) (GFP-4B and GFP-4B^{154}) (*SI Appendix*, Fig. S4*A*). Whereas the GFP-4B fusion protein could be readily detected in transduced wild-type MEFs and transiently transfected human 293T cells, the GFP-4B^{154} fusion protein was undetectable (*SI Appendix*, Fig. S4 *B* and *C*). Exposure of these cDNA-expressing cells to the proteasome inhibitor MG-132 also failed to identify GFP-4B^{154}, suggesting that the truncated KRAS4B^{154} protein may not properly fold and becomes degraded by a proteasome-independent mechanism (*SI Appendix*, Fig. S4*C*).

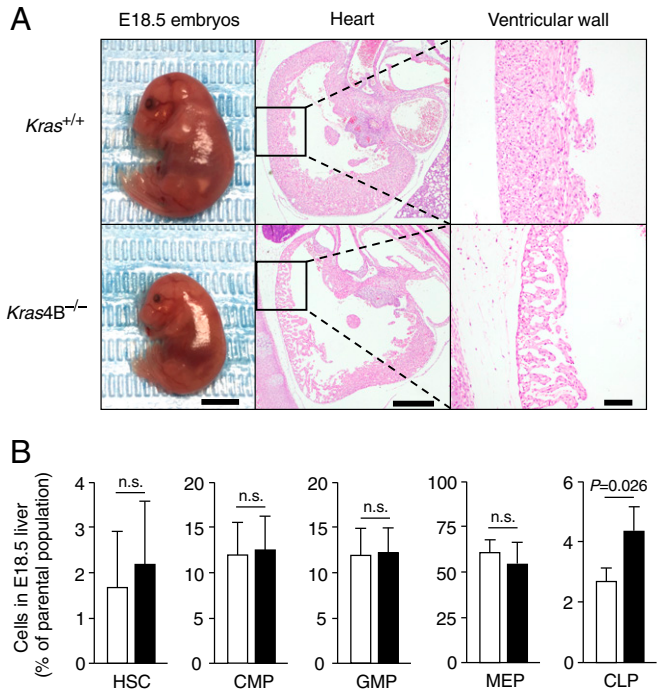

Fig. 2. Embryonic development of *Kras*4B$^{-/-}$ embryos. (*A*, *Left*) Representative images of *Kras*$^{+/+}$ and *Kras*4B$^{-/-}$ embryos at E18.5. (Scale bar, 5 mm.) (*A*, *Middle*) H&E staining of heart sections of *Kras*$^{+/+}$ and *Kras*4B$^{-/-}$ embryos at E18.5. (Scale bar, 500 μm.) (*A*, *Right*) Magnifications of the ventricular wall. (Scale bar, 100 μm.) (*B*) Frequencies of HSC, CMP, GMP, MEP, and CLP cell populations in livers of *Kras*$^{+/+}$ (open bars, $n = 3$) or *Kras*4B$^{-/-}$ (solid bars, $n = 3$) E18.5 embryos. Data are represented as mean ± SD. *P* values were calculated using the unpaired Student's *t* test. n.s., not significant.

KRAS4B^{154} Is Unstable because of an Incomplete α5-Helix. To further confirm the instability of the truncated KRAS4B^{154} polypeptide, we generated a series of GFP-4B deletion mutants lacking increasing residues of the C-terminal end including those forming the α5-helix (22) (Fig. 1*D* and *SI Appendix*, Fig. S5*A*). Whereas deletion of the HVR (GFP-4B^{174} and GFP-4B^{166}) had no detrimental effect on their expression levels, removal of 3 (GFP-4B^{163}), 7 (GFP-4B^{158}), or 10 (GFP-4B^{154}) amino acid residues from the α5-helix caused increasing protein instability, thus illustrating that the α5-helix is required for the stability of the KRAS4B isoform (*SI Appendix*, Fig. S5 *B* and *C*). We also quantified the amounts of GFP-4B, GFP-4B^{174}, GFP-4B^{158}, and GFP-4B^{154} after transfection into 293T cells by mass spectrometric analyses of peptides unique to KRAS or EGFP and observed that GFP-4B^{154} was expressed at 0.07 to 0.44% of GFP-4B (*SI Appendix*, *SI Materials and Methods* and Figs. S6*A*, S7, and S8), again confirming the instability of KRAS4B^{154}. To further rule out that any residual putative KRAS4B^{154} could act in a dominant-negative manner, we expressed these GFP-4B deletion mutants in RASless MEFs (23) and tested whether they could have a negative effect on the levels of colony formation induced by either wild-type KRAS4B or KRAS4B^{G12V}. As illustrated in *SI Appendix*, Fig. S6*B*, none of the GFP-4B deletion mutants had any significant effect on colony formation induced by wild-type KRAS4B or KRAS4B^{G12V} proteins in RASless MEFs. Consequently, the instability of the truncated KRAS4B^{154} protein underscores the fact that *Kras*4B^{-} is a bona fide null allele (Fig. 1*A*).

The relative expression levels of the KRAS4A isoform in *Kras*4B$^{-/-}$ MEFs were also determined by mass spectrometric analyses of peptides unique to this isoform along with two peptides common to both KRAS proteins (*SI Appendix*, Figs. S7 and S9). As illustrated in Fig. 3*C*, *Kras*4B$^{-/-}$ MEFs only expressed 3.5% of the amount of total KRAS protein present in their wild-type

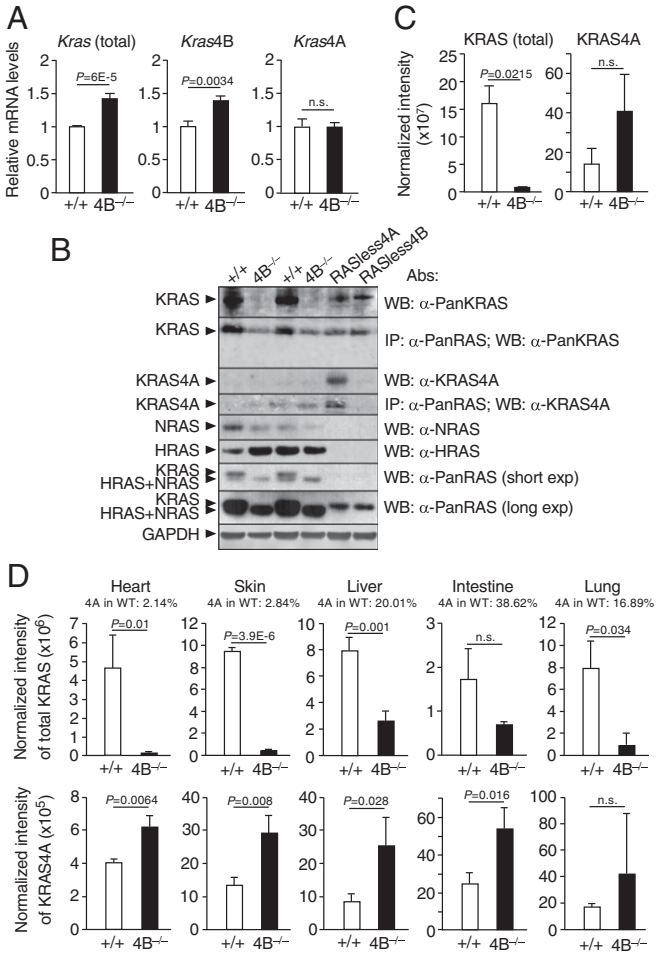

Fig. 3. Expression of KRAS4A and KRAS4B isoforms in *Kras*$^{+/+}$ and *Kras*4B$^{-/-}$ MEFs and tissues from newborn mice. (*A*) Relative expression levels of total *Kras*, *Kras*4B, or *Kras*4A mRNA in primary wild-type (+/+) (open bars, $n = 3$) or *Kras*4B$^{-/-}$ (4B$^{-/-}$) (solid bars, $n = 3$) MEFs. Data are represented as mean ± SD. *P* values were calculated using the unpaired Student's *t* test. n.s., not significant. (*B*) Western blot analysis of total KRAS, KRAS4A, HRAS, and NRAS expression in two independent primary wild-type (+/+) or *Kras*4B$^{-/-}$ (4B$^{-/-}$) MEF cultures. RASless MEFs ectopically expressing KRAS4A (RASless4A) or KRAS4B (RASless4B) were used as controls. GAPDH expression served as a loading control. Total KRAS and KRAS4A expression was determined by either Western blot analysis of immunoprecipitates obtained with anti-PanRAS antibodies or total cell extracts using anti-PanKRAS or anti-KRAS4A antibodies. Expression of NRAS or HRAS protein was analyzed by Western blotting of cell extracts using specific anti-NRAS or anti-HRAS antibodies, respectively. Expression of the three RAS proteins, KRAS, NRAS, and HRAS, was carried out by Western blot analysis of cell extracts using anti-PanRAS antibodies. A short and a long exposure are shown to better identify the three RAS proteins. Migration of the corresponding RAS proteins is indicated by arrowheads. Data are representative of three independent experiments. IP, immunoprecipitation; WB, Western blotting. (*C*) Relative quantification of the expression levels of total KRAS and KRAS4A proteins by label-free quantification in primary wild-type (+/+) (open bars) or *Kras*4B$^{-/-}$ (4B$^{-/-}$) (solid bars) MEFs. Data are represented as mean ± SD. *P* values were calculated using the unpaired Student's *t* test. n.s., not significant. The calculated percentage of KRAS4A with respect to total KRAS is also indicated. (*D*) Relative quantification of the expression levels of total KRAS and KRAS4A proteins by label-free quantification in the indicated tissues from wild-type (+/+) (open bars, $n = 3$) or *Kras*4B$^{-/-}$ (4B$^{-/-}$) (solid bars, $n = 3$; lung, $n = 2$) P0/P1 newborn mice. Data are represented as mean ± SD. *P* values were calculated using the unpaired Student's *t* test. n.s., not significant. The percentage of KRAS4A expression with respect to total KRAS protein is indicated.

counterparts. Since the truncated KRAS4B^{154} protein is unstable, the KRAS protein present in *Kras*4B$^{-/-}$ MEFs must correspond exclusively to the KRAS4A isoform. Interestingly, mass spectrometric analyses of peptides unique for KRAS4A revealed that the targeted MEFs expressed 2.9-fold more KRAS4A than wild-type MEFs (Fig. 3*C*). Together, these results indicate that in MEFs, the KRAS4B isoform represents most (98.28%) of the total KRAS protein. Similarly, we also determined the expression levels of KRAS4A and total KRAS in several tissues of either wild-type or *Kras*4B$^{-/-}$ newborn (P0/P1) mice (*SI Appendix*, Figs. S7 and S10). As illustrated in Fig. 3*D*, KRAS4A represents only 2.14% of total KRAS protein in the heart, thus suggesting that the defects in heart development in *Kras*4B$^{-/-}$ embryos likely arose as a consequence of the low KRAS4A expression levels. In contrast, tissues such as liver (20.01%) or intestine (38.62%) display significantly higher levels of KRAS4A expression.

Proliferative Properties of *Kras*4B$^{-/-}$ MEFs. Primary *Kras*4B$^{-/-}$ MEFs proliferated poorly and duplicated only once in 8 to 10 d, whereas MEFs obtained from wild-type littermates proliferated efficiently (Fig. 4*A*). Interestingly, the proliferation rate of primary MEFs lacking the entire *Kras* locus was indistinguishable from those lacking only KRAS4B expression, indicating that the low levels of KRAS4A present in these cells is not sufficient to compensate for the lack of KRAS4B protein in MEFs. Next, we analyzed the capacity of mitogen-activated protein kinase (MAPK) and phosphoinositide 3-kinase (PI3K)/protein kinase B (AKT) pathway activation following restimulation with serum in serum-starved wild-type as well as *Kras*4B$^{-/-}$ MEFs. As illustrated in Fig. 4*B*, the levels of phosphorylated extracellular signal-regulated kinase (ERK)1/2 proteins were significantly lower in serum-starved *Kras*4B$^{-/-}$ MEFs after restimulation with serum as compared with their wild-type littermates. Indeed, both the maximum intensity as well as the duration of ERK1/2 phosphorylation were diminished. The levels of phosphorylated AKT were also reduced, but less pronounced than those of phosphorylated ERK1/2.

Ectopic Expression of KRAS4A and KRAS4B Isoforms in RASless MEFs. To determine whether the limited proliferative properties of the *Kras*4B$^{-/-}$ MEFs were due to the low levels of expression of KRAS4A or to the inability of this isoform to sustain cell proliferation, we ectopically expressed both KRAS isoforms in *Kras*lox MEFs under the control of the same retroviral promotor. As indicated above, *Kras*lox cells do not express HRAS or NRAS and completely cease proliferation upon ablation of their conditional *Kras* alleles (23). As illustrated in Fig. 4*C*, ectopic expression of either KRAS4A or KRAS4B elicited similar levels of cell proliferation in *Kras*lox MEFs upon ablation of the endogenous *Kras* locus. Analysis of the MAPK pathway in those cells whose proliferation was exclusively driven by the KRAS4A or the KRAS4B isoform also revealed no significant differences (Fig. 4*D*). These results indicate that both KRAS protein isoforms have very similar properties. Thus, the limited proliferative properties of *Kras*4B$^{-/-}$ MEFs must be a consequence of the low levels of expression of the KRAS4A isoform.

Expression of a KRAS4A^{G12V} Isoform. Next, we examined whether the classical G12V mutation may selectively confer transforming properties to the KRAS4A isoform in the absence of KRAS4B^{G12V} protein expression. To this end, we generated another *Kras* allele by introducing the stop terminator sequences into codon 155 of the KRAS4B isoform directly into embryos derived from *Kras*$^{+/FSFG12V}$ mice (24) as described above. Mice carrying this targeting event in the *Kras*^{FSFG12V} allele, designated *Kras*$^{FSF4AG12V4B-}$, selectively express a KRAS4A^{G12V} mutant protein upon optimized flippase (FLPo)-mediated recombination (Fig. 5*A*). Proper development and survival of these mice were guaranteed by the presence of the wild-type *Kras* allele.

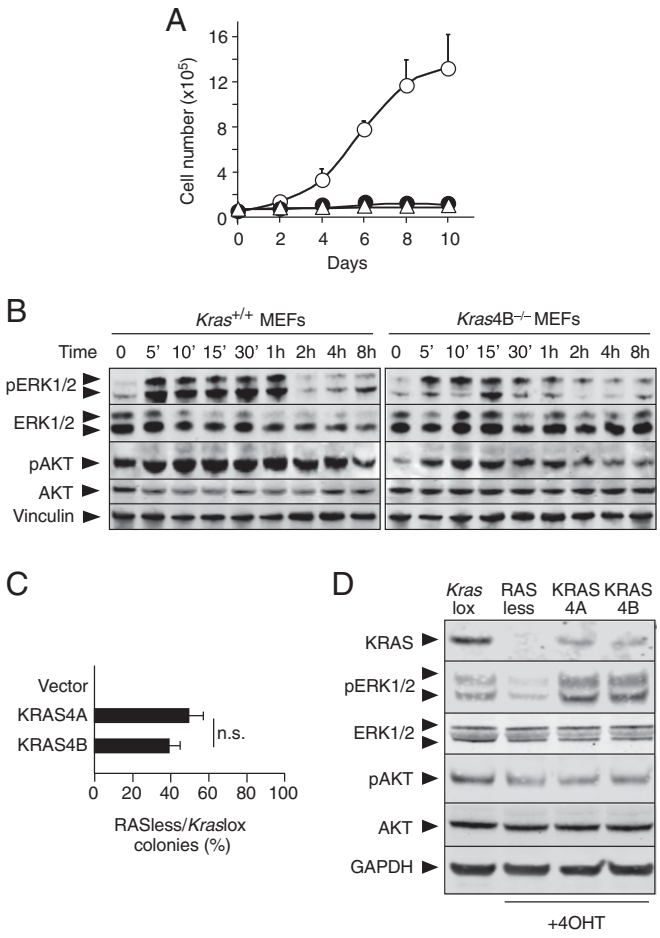

Fig. 4. Growth properties of *Kras*4B$^{-/-}$ MEFs. (*A*) Proliferation of primary *Kras*$^{+/+}$ (open circles), *Kras*4B$^{-/-}$ (closed circles), or *Kras*$^{-/-}$ (open triangles) MEFs. Data are represented as mean ± SD. (*B*) Western blot analysis of pERK1/2, total ERK1/2, pAKT, and total AKT expression in serum-starved primary *Kras*$^{+/+}$ (*Left*) or *Kras*4B$^{-/-}$ (*Right*) MEFs restimulated with 10% FBS for the indicated times. Vinculin expression served as a loading control. The data are representative of three independent experiments. (*C*) Colony formation of *Kras*lox and RASless MEFs infected with the indicated cDNAs and expressed as the ratio between the number of colonies observed in cells lacking endogenous RAS proteins (RASless) and those expressing KRAS (*Kras*lox). Data are represented as mean ± SD. *P* values were calculated using the unpaired Student's *t* test. n.s., not significant. (*D*) Western blot analysis of KRAS, pERK1/2, total ERK1/2, pAKT, and total AKT expression in untreated *Kras*lox MEFs, or *Kras*lox MEFs exposed to 4-hydroxytamoxifen (4OHT) to eliminate expression of the endogenous *Kras* alleles followed by infection with empty retroviruses (RASless) or with retroviruses expressing KRAS4A or KRAS4B cDNAs. GAPDH expression served as a loading control. The data are representative of three independent experiments.

To analyze the consequences of selectively expressing a mutant KRAS4A^{G12V} protein from the endogenous *Kras* locus in the absence of the KRAS4B^{G12V} isoform, we generated MEFs from *Kras*$^{+/FSF4AG12V4B-}$ and *Kras*$^{+/FSFG12V}$ E13.5 embryos. Previous studies have shown that MEFs expressing both oncogenic KRAS^{G12V} isoforms from their endogenous locus do not become morphologically transformed but proliferate as immortal cells without undergoing replicative senescence (25). Hence, we infected *Kras*$^{+/FSF4AG12V4B-}$ and *Kras*$^{+/FSFG12V}$ MEFs with Adeno-FLPo to induce expression of either KRAS4A^{G12V} alone, or both KRAS4A^{G12V} and KRAS4B^{G12V} mutant isoforms, respectively. As controls, cells were infected with Adeno-GFP. As illustrated in Fig. 5*B*, *Kras*$^{+/FSFG12V}$ MEFs infected with Adeno-FLPo exhibited continuous exponential growth without displaying replicative senescence, as previously reported for *Kras*$^{+/LSLG12V}$ MEFs after Cre-mediated recombination (25). In contrast, *Kras*$^{+/FSF4AG12V4B-}$ MEFs infected with Adeno-FLPo entered into replicative senescence following kinetics similar to those of control *Kras*$^{+/FSFG12V}$ MEFs infected with Adeno-GFP. These observations indicate that expression of the endogenous KRAS4A^{G12V} mutant isoform, in the absence of KRAS4B^{G12V}, is not sufficient to prevent replicative senescence in MEFs. Quantification of the levels of expression of these mutant proteins using a G12V selective peptide revealed that the amount of KRAS4A^{G12V} present in Adeno-FLPo–infected *Kras*$^{+/FSF4AG12V4B-}$ MEFs was only 5.25% of the total KRAS^{G12V} protein present in Adeno-FLPo–infected *Kras*$^{+/FSFG12V}$ MEFs (Fig. 5*C* and *SI Appendix*, Figs. S7 and S11). These levels of expression may explain the shorter duration and lower levels of ERK1/2 phosphorylation in *Kras*$^{+/FSF4AG12V4B-}$ MEFs when compared with *Kras*$^{+/FSFG12V}$ MEFs upon Adeno-FLPo infection and consequently its inability to overcome replicative senescence (Fig. 5*D*).

Transforming Properties of the KRAS4A^{G12V} Mutant Isoform. To determine whether these results were a consequence of an intrinsic inability of the KRAS4A^{G12V} mutant isoform to overcome cellular senescence or whether, as illustrated above, this was a consequence of its limited levels of expression in MEFs, we ectopically expressed the KRAS4A^{G12V} and KRAS4B^{G12V} in *Kras*lox cells under the control of the same promoter in the absence of endogenous RAS proteins. As illustrated in Fig. 5*E* and *SI Appendix*, Fig. S12, both isoforms induced similar levels of colony formation in RASless cells. Moreover, KRAS4A^{G12V} even displayed a more potent transforming activity than KRAS4B^{G12V} when expressed in NIH 3T3 cells (Fig. 5*F*). These results, taken together, strongly suggest that the limited ability of *Kras*$^{+/4AG12V4B-}$ MEFs to overcome replicative senescence must be a consequence of its low levels of expression, since both KRAS isoforms display similar properties when expressed at comparable expression levels, at least in vitro.

KRAS4A^{G12V} Drives Lung Tumor Formation. Therefore, we decided to interrogate whether expression of the mutant KRAS4A^{G12V} isoform was sufficient to induce lung tumor formation by itself in mice. To this end, we added *p53*$^{frt/frt}$ (*p53*$^{F/F}$) alleles to *Kras*$^{+/FSF4AG12V4B-}$ mice to facilitate tumor induction and to better compare the results with previous studies using expression of both KRAS mutant isoforms. As expected, intranasal inoculation of control *Kras*$^{+/FSFG12V}$;*p53*$^{F/F}$ mice with Adeno-FLPo resulted in the death of all the animals due to lung cancer with a median survival time of 13 wk (Fig. 6*A*). Interestingly, *Kras*$^{+/FSF4AG12V4B-}$;*p53*$^{F/F}$ mice submitted to the same treatment also developed lung tumors with 100% penetrance. Yet, their median survival time was approximately three times longer.

The lungs of *Kras*$^{+/FSF4AG12V4B-}$;*p53*$^{F/F}$ mice, examined at a humane end point, displayed multiple tumors that presented similar levels of phosphorylated ERK1/2 as those present in control *Kras*$^{+/FSFG12V}$;*p53*$^{F/F}$ mice (Fig. 6*B*). On average, *Kras*$^{+/FSFG12V}$;*p53*$^{F/F}$ mice developed 89.2 lesions whereas *Kras*$^{+/FSF4AG12V4B-}$;*p53*$^{F/F}$ mice only developed 26.9 lesions at their respective humane end points (Fig. 6*C*). Despite these differences, the distribution of tumor grades (26) in lesions found in *Kras*$^{+/FSF4AG12V4B-}$;*p53*$^{F/F}$ or *Kras*$^{+/FSFG12V}$;*p53*$^{F/F}$ animals was similar (*SI Appendix*, Fig. S13*A*). Interestingly, *Kras*$^{+/FSF4AG12V4B-}$ mice carrying wild-type *p53* alleles also displayed lung tumors when they were killed 1 y after infection with Adeno-FLPo (*SI Appendix*, Fig. S14).

To ascertain whether the differential tumor latency was due to lower levels of expression of the KRAS4A^{G12V} isoform, we determined the levels of expression of KRAS^{G12V} oncoproteins by mass spectrometry in cell lines obtained from tumors isolated from *Kras*$^{+/FSF4AG12V4B-}$;*p53*$^{F/F}$ or *Kras*$^{+/FSFG12V}$;*p53*$^{F/F}$ mice.

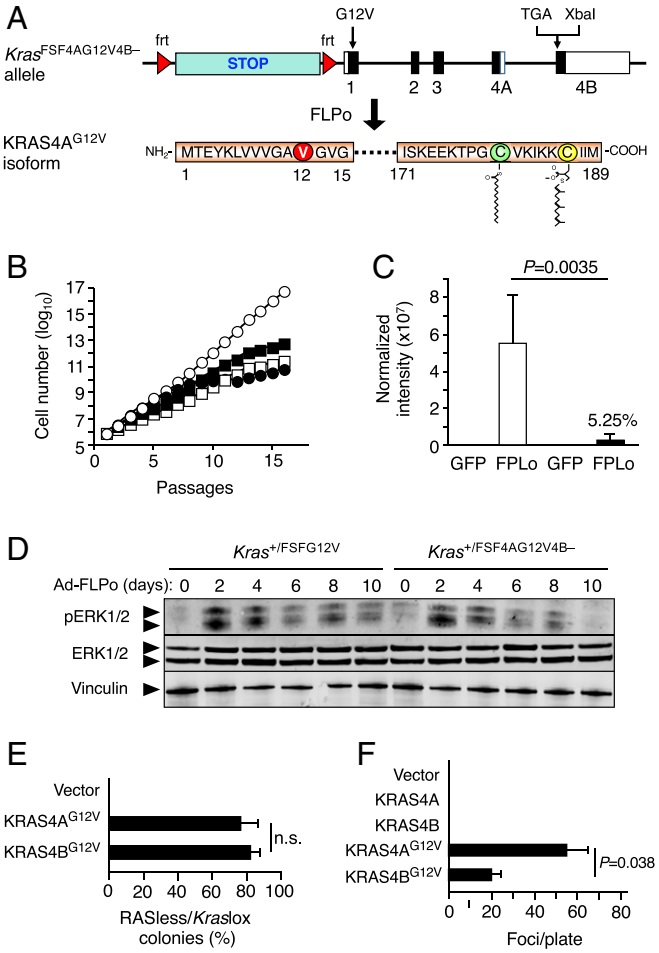

Fig. 5. In vitro properties of the mutant KRAS4A^{G12V} isoform. (*A*) Generation of the *Kras*$^{FSF4AG12V4B–}$ allele by gene editing of a conditional *Kras*^{FSFG12V} allele. (*A*, *Top*) Genomic structure. Exons are indicated by numbered boxes. Noncoding sequences appear as open boxes. Coding sequences are shown by solid boxes. The engineered stop codon (TGA) and the diagnostic XbaI restriction sites introduced into exon 4B are indicated. The transcriptional STOP cassette is shown as a green box and *frt* sequences as red triangles. The G12V mutation in exon 1 is indicated by an arrow. (*A*, *Bottom*) Protein sequence of the KRAS4A^{G12V} (amino acids 1 to 15 and 171 to 189) isoform generated after FLPo-mediated recombination of the *Kras*$^{FSF4AG12V4B–}$ allele. The Val12 residue is indicated as a red circle. Palmitoylated Cys180 and farnesylated Cys186 residues are indicated by a green and yellow circle, respectively. (*B*) Immortalization of primary *Kras*$^{+/FSFG12V}$ (circles) or *Kras*$^{+/FSF4AG12V4B–}$ MEFs (squares) after infection with Adeno-GFP (solid symbols) or Adeno-FLPo (open symbols) following a 3T3 protocol. (*C*) Relative quantification of the expression levels of total KRAS oncoproteins by label-free quantification in *Kras*$^{+/FSFG12V}$ (open bars, $n = 2$) or *Kras*$^{+/FSF4AG12V4B–}$ (solid bars, $n = 3$) MEFs after infection with Adeno-GFP or Adeno-FLPo obtained at passage 10. Data are represented as mean ± SD. *P* values were calculated using the unpaired Student's *t* test. (*D*) Western blot analysis of pERK1/2 and ERK1/2 expression in primary *Kras*$^{+/FSFG12V}$ or *Kras*$^{+/FSF4AG12V4B–}$ MEFs infected with Adeno-FLPo for the indicated days. Vinculin expression served as a loading control. (*E*) Colony formation of RASless and *Kras*lox MEFs infected with either empty vector or vectors containing cDNAs encoding KRAS4A^{G12V} or KRAS4B^{G12V} mutant isoforms expressed as the ratio between the number of colonies observed in cells lacking endogenous RAS proteins (RASless) and those expressing KRAS (*Kras*lox). Data are represented as mean ± SD. *P* values were calculated using the unpaired Student's *t* test. n.s., not significant. (*F*) Transformation of NIH 3T3 cells transfected with empty vector or vectors containing cDNAs encoding KRAS4A, KRAS4B, KRAS4A^{G12V}, or KRAS4B^{G12V} isoforms (1 μg) represented as the number of foci per plate. Data are represented as mean ± SD. *P* values were calculated using the unpaired Student's *t* test.

As illustrated in Fig. 6*D*, the levels of expression of the KRAS4A^{G12V} isoform in cells derived from *Kras*$^{+/FSF4AG12V4B–}$;*p53*$^{F/F}$ tumors were 36% of those of total KRAS^{G12V} proteins present in the corresponding tumor cells derived from control *Kras*$^{+/FSFG12V}$;*p53*$^{F/F}$ animals in which both oncogenic KRAS isoforms are present. These levels of KRAS4A^{G12V} expression compared with total KRAS^{G12V} protein were considerably higher than those observed in MEFs, an observation that might explain the ability of the recombined *Kras*$^{4AG12V4B–}$ allele to induce lung tumors. This oncogenic activity was also facilitated by the increased levels of allele amplification of the targeted *Kras*$^{4AG12V4B–}$ allele versus the *Kras*^{G12V} allele (Fig. 6*E*).

Finally, 20% of *Kras*$^{+/FSF4AG12V4B–}$;*p53*$^{F/F}$ mice developed local metastases to lymph nodes or heart tissue, a phenomenon not observed in control *Kras*$^{+/FSFG12V}$;*p53* $^{F/F}$ animals (Fig. 7 *A* and *B*). Whole-exome sequencing of these lesions did not reveal mutations significantly associated with tumor formation or metastatic invasion (Fig. 7*C* and Dataset S1). Moreover, we did not detect additional driver mutations in both primary and metastatic tumors from *Kras*$^{+/FSF4AG12V4B–}$;*p53*$^{F/F}$ mice, suggesting that KRAS4A^{G12V} was the sole driver of these lesions (Fig. 7*C* and Dataset S1).

Interestingly, *Kras*$^{+/4AG12V4B–}$;*p53*$^{–/–}$ tumor cells had a similar proliferation rate as those *Kras*$^{+/G12V}$;*p53*$^{–/–}$ tumor cells that express both isoforms, under both low and optimal serum concentrations (*SI Appendix*, Fig. S15*A*). Moreover, *Kras*$^{+/4AG12V4B–}$;*p53*$^{–/–}$ tumor cells displayed higher levels of ERK1/2 phosphorylation (*SI Appendix*, Fig. S15*B*), thus adding further evidence that the limited biological activity observed for the KRAS4A isoform in certain scenarios is not a consequence of its intrinsic signaling properties but of its lower levels of expression. In summary, our results demonstrate that KRAS4A^{G12V} is a bona fide oncoprotein that, when expressed at levels not too dissimilar from those of the KRAS4B^{G12V} isoform (36 vs. 64% of the total KRAS^{G12V} protein), is sufficient to license lung tumor formation in the absence of the KRAS4B^{G12V} isoform.

Discussion

The biological relevance of the expression of two KRAS isoforms exhibiting distinct carboxyl-terminal domains has puzzled researchers for decades. It has been argued that these isoforms display distinct modes of membrane attachment and trafficking between different membrane compartments (4–6). In addition, the expression levels of KRAS4A and KRAS4B vary profoundly throughout different tissues and developmental stages (10, 17, 18). However, genetic analyses have failed to identify selective requirements for KRAS4A and KRAS4B during normal cell proliferation (ref. 23 and this study). Whereas germline ablation of the KRAS4A isoform does not appear to have deleterious consequences for embryonic development or adult homeostasis, the effect of selective elimination of the KRAS4B isoform remained to be explored. Knockin of either KRAS4A or KRAS4B cDNAs into the *Kras* locus supports embryonic development and adult homeostasis, indicating that both isoforms are able to perform similar functions in some contexts (27). In addition, replacement of *Kras* with an HRAS cDNA also supports normal embryonic development despite causing dilated cardiomyopathy and arterial hypertension later in life (28). Yet, the appearance of these cardiovascular defects can be prevented by reducing the number of *Hras* alleles in these mice from four to two by ablation of the endogenous *Hras* locus (29), thus indicating that most RAS isoforms can perform similar tasks during development despite the differences in their HVR and that their main difference, albeit not all, is mediated by their pattern of expression.

In this study, we selectively disrupted expression of the KRAS4B isoform by inserting a premature termination codon into its coding sequences that prevented expression of its 34 carboxyl-terminal residues, a region that encompassed most of the α5-helix,

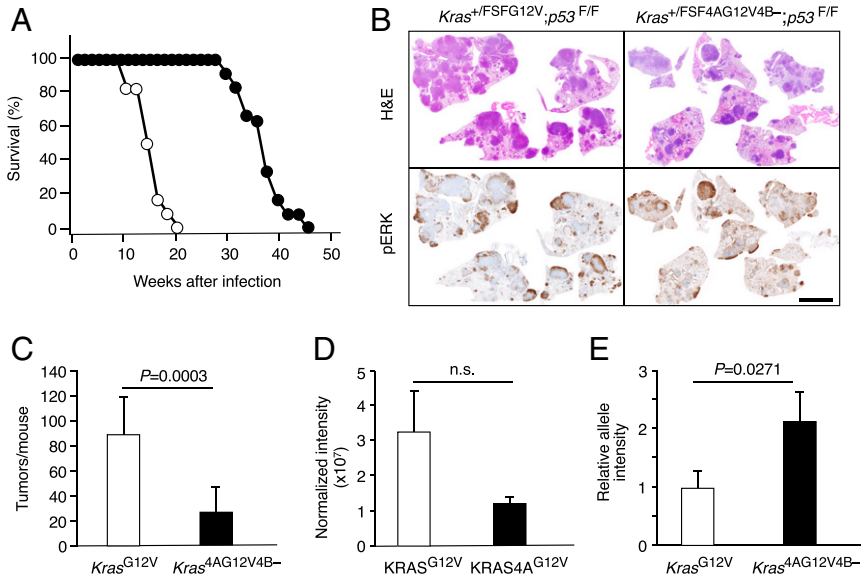

Fig. 6. Induction of lung tumors upon expression of an endogenous KRAS4A^{G12V} mutant isoform. (*A*) Survival of *Kras*$^{+/FSFG12V}$;*p53*$^{F/F}$ (open circles, $n = 12$) or *Kras*$^{+/FSF4AG12V4B-}$;*p53*$^{F/F}$ mice (solid circles, $n = 12$) infected with 10^8 plaque-forming units (pfu) Adeno-FLPo at 8 wk of age. (*B*) Representative images of consecutive lung sections stained with H&E (*Top*) or after IHC staining with anti-pERK antibodies (*Bottom*) obtained from *Kras*$^{+/FSFG12V}$;*p53*$^{F/F}$ or *Kras*$^{+/FSF4AG12V4B-}$;*p53*$^{F/F}$ mice infected with 10^8 pfu Adeno-FLPo and killed at a humane end point. (Scale bar, 5 mm.) (*C*) Average number of tumors per mouse in lungs obtained from *Kras*$^{+/FSFG12V}$;*p53*$^{F/F}$ (open bars, $n = 6$) or *Kras*$^{+/FSF4AG12V4B-}$;*p53*$^{F/F}$ mice (solid bars, $n = 9$) infected with 10^8 pfu Adeno-FLPo and killed at a humane end point. Data are represented as mean ± SD. *P* values were calculated using the unpaired Student's *t* test. (*D*) Relative quantification of the levels of expression of total KRAS^{G12V} oncoproteins by label-free quantification in cell lines obtained from *Kras*$^{+/FSFG12V}$;*p53*$^{F/F}$ (open bars, $n = 2$) or *Kras*$^{+/FSF4AG12V4B-}$;*p53*$^{F/F}$ mice (solid bars, $n = 3$) infected with 10^8 pfu Adeno-FLPo and killed at a humane end point. Data are represented as mean ± SD. *P* values were calculated using the unpaired Student's *t* test. n.s., not significant. (*E*) Relative levels of oncogenic *Kras* alleles determined by semiquantitative PCR in lung tumors obtained from *Kras*$^{+/FSFG12V}$;*p53*$^{F/F}$ (open bars, $n = 3$) or *Kras*$^{+/FSF4AG12V4B-}$;*p53*$^{F/F}$ mice (solid bars, $n = 3$) infected with 10^8 pfu Adeno-FLPo and killed at a humane end point. The intensity of PCR bands was quantified and normalized to the intensity of the *Pdcd1* locus on mouse chromosome 1. Data are represented as mean ± SD. *P* values were calculated using the unpaired Student's *t* test.

the HVR, as well as the CAAX domain. Moreover, this truncated protein is highly unstable and could not be detected in any of the cells or tissues explored due to the absence of most amino acids required to form the α5-helix. The hydrophobic face of this helix makes direct contacts with β-sheets 1 to 3 presumably required to stabilize the G domain of KRAS4B (30). Since this mutation did not affect either transcription or translation of the KRAS4A isoform, we conclude that the strain described here is a bona fide *Kras*4B-null mutant.

Lack of KRAS4B expression causes developmental defects incompatible with postnatal life. Our results are reminiscent of those obtained when disrupting the entire *Kras* locus (14, 15), although most *Kras*4B-null embryos develop to term rather than die during midgestation. We observed a general growth retardation as well as hypertrabeculation of the ventricular wall indicative of defective myocardial compaction. Interestingly, KRAS4B appears to be the major KRAS isoform expressed in the heart (97.9%), thus suggesting that these defects could be a consequence of an almost complete reduction of KRAS expression in this organ (17). In contrast, we were unable to detect other phenotypes described in *Kras*-null embryos such as fetal liver apoptosis, which suggests that the remaining expression levels of KRAS4A are sufficient to prevent these phenotypes. Moreover, we observed that KRAS4A only constitutes 1.7% of the total KRAS levels in MEFs. Thus, it was not surprising to observe a striking similarity between *Kras*4B$^{-/-}$ and *Kras*-null MEFs in proliferation. Moreover, lack of KRAS4B expression results in defective MAPK signaling, thus suggesting that both KRAS isoforms are required for optimal MAPK signaling and proliferation in MEFs. Taken together, our results indicate that expression of the endogenous KRAS4B isoform, in contrast to KRAS4A, is strictly required for mouse development.

Human tumors appear to express both isoforms, albeit to varying degrees (10, 18, 19). Yet, the relative impact of each isoform in tumor development or progression is unclear. Genetic experiments have proposed that lack of KRAS4A significantly impedes tumor formation in a chemical carcinogenesis model of lung cancer (20). Somewhat surprisingly, expression of either the KRAS4A or the KRAS4B cDNA from the endogenous *Kras* locus rendered mice largely resistant to chemical lung carcinogenesis (21, 27). In this study, we have shown that activation of a resident *Kras*^{G12V} allele in the absence of KRAS4B expression is sufficient to drive lung tumor formation, although tumors appeared significantly later and with lower incidence than those expressing both oncoproteins. These results suggest that KRAS4A^{G12V}, when expressed under conditions maintaining its natural regulation, including its endogenous promoter as well as its exon/intron composition, is capable of inducing lung cancer growth by itself. Interestingly, in agreement with a previous study (31), we observed that KRAS4A^{G12V} has a slightly higher transforming capacity than KRAS4B^{G12V} in NIH 3T3 cells. Interestingly, mice that selectively express the KRAS4A mutant isoform elicited proximal metastasis in 20% of the animals, a feature seldom observed in mice expressing both oncogenic isoforms. Whether these observations are a consequence of the longer latency of those tumors exclusively driven by the KRAS4A^{G12V} oncogenic isoform remains to be resolved. Yet, we did not observe any significant enrichment for mutations in other driver oncogenes or tumor suppressors after selective expression of KRAS4A^{G12V} that could independently induce lung tumor formation or metastasis, thus suggesting that these processes were driven solely by KRAS4A^{G12V}.

A more recent study that examined the interactomes of KRAS4A and KRAS4B also identified a stronger transforming capability of KRAS4A consistent with stronger activation of

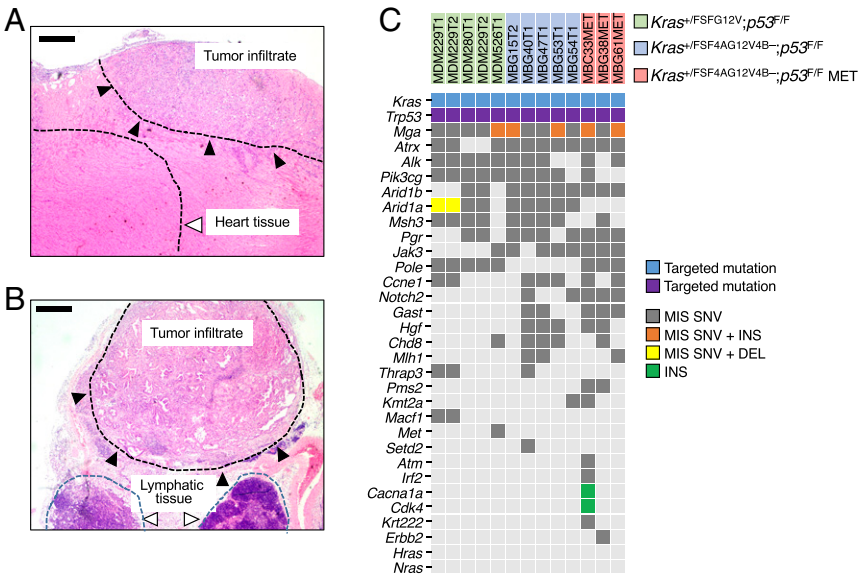

Fig. 7. Expression of the KRAS4A^{G12V} mutant isoform induces metastatic lesions in *Kras*$^{+/FSF4AG12V4B-}$;*p53*$^{F/F}$ mice. (*A*) Representative image of a metastasis to the heart. (Scale bar, 500 μm.) Solid arrowheads indicate metastatic tumor tissue. Healthy heart tissue is indicated by an open arrowhead. (*B*) Representative image of a local metastasis to a lymph node. (Scale bar, 500 μm.) Solid arrowheads indicate metastatic tumor tissue. Healthy lymphatic tissue is indicated by open arrowheads. (*C*) Representative mutations in genes described to be altered in lung adenocarcinoma as determined by whole-exome sequencing of formalin-fixed paraffin-embedded tumors obtained from *Kras*$^{+/FSFG12V}$;*p53*$^{F/F}$ mice (green, $n = 5$) or *Kras*$^{+/FSF4AG12V4B-}$;*p53*$^{F/F}$ mice (light blue, $n = 5$), or metastatic lesions from *Kras*$^{+/FSF4AG12V4B-}$;*p53*$^{F/F}$ mice (orange, $n = 3$). Targeted mutations in *Kras* and *p53* loci are indicated in blue and purple, respectively. Somatic mutations including missense single-nucleotide variants (MIS SNV; dark gray), missense single-nucleotide variant + insertion (MIS SNV + INS; orange), missense single-nucleotide variant + deletion (MIS SNV + DEL; yellow), and insertion (INS; green) are also indicated. The full list of variants is indicated in Dataset S1.

MAPK signaling (32). Moreover, mutant KRAS4A also induced higher ERK1/2 phosphorylation in a model of liver transgenesis which resulted in increased expression of p16 and consequently fewer tumors (33). These observations might explain why lower levels of KRAS4A^{G12V}, as compared with those of KRAS4B^{G12V}, are sufficient to induce tumorigenesis in vivo. These differences might propose a model in which cells are able to actively regulate inclusion/exclusion of exon 4A to adapt to specific situations (27).

Our data also suggest that expression levels of KRAS4A^{G12V} must nevertheless exceed a certain threshold of expression to facilitate lung tumor formation. Indeed, we observed higher levels of amplification of the *Kras* locus in tumors lacking KRAS4B, suggesting that natural selection processes provoked optimal, or at least sufficient, expression levels of KRAS4A oncoproteins to drive lung tumor formation. Finally, our results raise a note of caution regarding the development of therapeutic strategies selectively targeting KRAS4B mutant isoforms (34). Likewise, selective interference with KRAS4A oncoproteins, for instance by targeting selective effectors such as HK1 (13), might not result in effective antitumor responses either. Hence, the data presented here suggest that only those strategies aimed at blocking both KRAS isoforms may result in successful therapeutic strategies (35, 36).

Materials and Methods

CRISPR-Cas9 Microinjection. To generate mice lacking expression of the endogenous KRAS4B isoform, we used a single-stranded oligonucleotide (ssODN) template to introduce a TGA stop codon at nucleotides 13 to 15 of exon 4B along with an XbaI restriction site for screening purposes (*SI Appendix*, Fig. S1) through CRISPR-Cas9–guided homologous recombination. CRISPR-Cas9 reagents were microinjected into pronuclei of zygotes from superovulated F1 (C57BL/6.CBA) females crossed with *Kras*$^{+/FSFG12V}$;*p53*$^{F/F}$ males (24) on a mixed 129/Sv-C57BL/6 genetic background on the day of vaginal plug visualization (E0.5). A total of 334 zygotes were microinjected with a mix of ribonucleoprotein (30 ng/mL recombinant Cas9 protein, 20 ng/mL cr/trac CRISPR RNA, 10 ng/mL ssODN) in microinjection buffer (10 mM Tris, 0.1 mM ethylenediaminetetraacetate [EDTA], pH 8). All CRISPR reagents were purchased from IDT. After 24 h of incubation, zygotes that progressed to the two-cell stage (212 total) were transferred to the oviducts of pseudopregnant CD1 female mice (pE0.1). A total of 31 pups were born and 8 scored positive for integration of the XbaI restriction site at the desired position, 5 of which contained the targeted mutation in the *Kras*^{FSFG12V} allele. *Kras*$^{+/+}$ mice carrying the XbaI site were further crossed to wild-type 129/Sv-C57BL/6 mice to confirm that the homologous recombination event went into the germ line and these mice were designated *Kras*4B$^{+/-}$. *Kras*$^{+/FSFG12V}$;*p53*$^{+/F}$ mice scoring positive for integration of the XbaI site were further crossed with *p53*$^{+/F}$ mice to identify those mice in which the recombination event occurred in the allele that carried the FSFG12V cassette. These mice were designated *Kras*$^{+/FSF4AG12V4B-}$ since elimination of the FSF cassette via exposure to the FLPo recombinase resulted in the selective expression of the KRAS4A^{G12V} oncoprotein.

Mice. *Kras*4B$^{+/-}$ and *Kras*$^{+/FSF4AG12V4B-}$ mice were maintained on a mixed 129/Sv-C57BL/6 genetic background. *p53*^{F} mice have been described (37). All animal experiments were approved by the Ethical Committees of the Spanish National Cancer Research Centre, Carlos III Health Institute, and Autonomous Community of Madrid, and were performed in accordance with the guidelines stated in the International Guiding Principles for Biomedical Research Involving Animals, developed by the Council for International Organizations of Medical Sciences.

PCR Genotyping. To genotype the *Kras*$^{+}$, *Kras*4B^{-}, or *Kras*$^{FSF4AG12V4B-}$ alleles, we amplified a 520-nt DNA fragment with forward (5′-TTCTTAAGCCCATTCGGTTGCCAA-3′) and reverse (5′-GCATGCACCAAATCCCAAGACAG-3′) primers using DreamTaq PCR Master Mix under the following conditions: 2 min at 94 °C, 30 s at 94 °C, 30 s at 60 °C, 30 s at 72 °C (35 cycles), 5 min at 72 °C. The PCR products were subsequently purified with the QIAquick PCR Purification Kit (Qiagen). Digestion with XbaI resulted in DNA fragments of 345 and 175 base pairs in the case of the *Kras*4B^{-} or *Kras*$^{FSF4AG12V4B-}$ alleles as outlined in *SI Appendix*, Fig. S1.

Cell Lines and Retroviral Infection. MEFs were extracted from E13.5 embryos and cultured in Dulbecco's modified Eagle's medium (DMEM) supplemented with 10% fetal bovine serum (FBS). *Kras*lox MEFs have been described (23). NIH 3T3 cells were maintained in DMEM supplemented with 10% calf serum. Retroviral vectors expressing EGFP-KRAS4B were generated by amplifying

the cDNA of the EGFP-KRAS4B fusion protein, a gift from I. Perez de Castro, Instituto de Salud Carlos III, Madrid, Spain, by PCR and cloning into the EcoRI restriction site of pWZLblast. To generate the truncated EGFP-KRAS4B^{174} (GFP-4B^{174}), EGFP-KRAS4B^{166} (GFP-4B^{166}), EGFP-KRAS4B^{163} (GFP-4B^{163}), EGFP-KRAS4B^{158} (GFP-4B^{158}), or EGFP-KRAS4B^{154} (GFP-4B^{154}) proteins, we introduced a TGA stop codon at positions 175, 167, 164, 159, or 155, respectively, by site-directed mutagenesis using the QuikChange Lightning Site-Directed Mutagenesis Kit (Agilent). pBABEpuro KRAS4B and pBABEpuro KRAS4B^{G12V} have been described previously (23). They were used to replace the carboxyl-terminal sequences of KRAS4B with those of KRAS4A by cutting the vectors with EcoRI/SalI and introducing the corresponding PCR-generated sequences from KRAS4A in-frame using the In-Fusion HD EcoDry Cloning Kit (Takara Bio USA). All constructs were verified by sequencing. Retroviruses were produced with the pCL-Eco packaging vector as described (23).

Histopathology and Immunohistochemistry. For histological analyses, tissues were fixed in 10% neutral-buffered formalin and embedded in paraffin. Hematoxylin & eosin (H&E) staining as well as immunohistochemistry (IHC) analyses were performed on 3-μm paraffin sections. For IHC, the following antibodies were used: pERK (Pharmingen; 553057), Ki67 (Master Diagnostica; 0003110QD), or active caspase 3 (Cell Signaling; 9661).

Western Blot Analysis. Cells were lysed in 50 mM Tris·HCl (pH 7.4), 150 mM NaCl, 0.5% Nonidet P-40 supplemented with Complete Mini Protease Inhibitor Mixture (Roche), and phosphatase inhibitor mixtures 2 and 3 (Sigma). Usually, 40 μg of total protein lysate was separated by sodium dodecyl sulfate/polyacrylamide-gel electrophoresis and transferred to nitrocellulose membranes. Antibodies raised against the following proteins were used: Pan RAS (Calbiochem; OP40 [1:250]), Pan KRAS (Santa Cruz Biotechnology; sc-30 [1:200]), KRAS4A (EMD Millipore; ABC1442 [1:250]), HRAS (BD Transduction Laboratories; 610002 [1:500]), NRAS (Santa Cruz Biotechnology; sc-31 [1:200]), ERK1 (BD Pharmingen; 554100 [1:1,000]), ERK2 (BD Biosciences; 610103 [1:1,000]), pERK1/2 (Cell Signaling; 9101 [1:250]), AKT (Cell Signaling; 9272 [1:1,000]), pAKT (Cell Signaling; 9271 [1:250]), EGFP (Abcam; ab290 [1:1,000]), glyceraldehyde 3-phosphate dehydrogenase (GAPDH) (Sigma; G8795 [1:10000]), and vinculin (Sigma; V9131 [1:10000]). For immunoprecipitations, 500 μg total protein lysates was incubated with 1 μg α-Pan RAS antibodies (Calbiochem; OP40) overnight on a rotating wheel. The next day, proteins were precipitated for 2 h with 50 μL TrueBlot α-mouse agarose beads (Rockland), washed three times with Nonidet P-40 lysis buffer (see above), and resuspended in 30 μL 2× sample loading buffer.

Immunofluorescence Staining. Cells were seeded on glass coverslips, fixed with 4% paraformaldehyde, and permeabilized with 0.5% Triton X-100 for 5 min. Coverslips were blocked in phosphate-buffered saline (PBS) with 3% (weight/volume) bovine serum albumin (BSA) for 45 min and incubated with anti-EGFP antibodies (Abcam; ab290 [1:100]) in PBS with 3% BSA for 1 h. Coverslips were washed three times with PBS for 5 min and incubated with goat anti-rabbit Alexa Fluor 488 secondary antibodies (1:200) for 45 min in PBS with 3% BSA. Coverslips were washed again three times with PBS for 5 min and the nuclei were counterstained with Hoechst 33342. Finally, cells were imaged with a Leica TCS SP5 confocal microscope.

qRT-PCR Analysis. RNA was extracted using TRIzol (Life Technologies). Total RNA (1 μg) was reverse-transcribed using SuperScript II Reverse Transcriptase (Invitrogen) and random primers (Invitrogen) following the manufacturer's instructions. The qRT-PCR assays were performed with a FAST7500 Real-Time PCR System using Power SYBR Green PCR Master Mix (Applied Biosystems). Calculations for the values were made using the comparative threshold cycle (ΔΔCt) method. β-Actin was used for normalization. The forward (F) and reverse (R) primers utilized are shown in Table 1.

Flow Cytometry Analysis. Livers were collected from E18.5 embryos and single-cell suspensions were obtained by mechanical dissociation in RPMI 1640. Erythrocytes were lysed with ACK lysis buffer (Lonza) and cells were incubated with 3% BSA in PBS for 5 min at room temperature to block Fc receptors. Cells were resuspended in PBS containing 0.1% BSA and 2 mM EDTA, and aliquots of 3×10^6 cells were stained for 1 h on ice with the following monoclonal antibodies: Alexa Fluor 488 α-CD127 (IL7Rα) (1:200), APC mouse lineage antibody mixture (1:100), APC-H7 α-CD117 (c-Kit) (1:200), PE-Cy7 α-CD16/32 (FcγR) (1:400), PE α-CD34 (1:50), and PerCP-Cy5.5 α-Ly-6A/E (Sca-1) (1:200). DAPI was used to identify dead cells. Samples were processed on a FACSCanto II flow cytometer (BD Pharmingen) and data were analyzed using FlowJo (Tree Star). Hematopoietic stem cells (HSCs) were gated as Lin$^-$/IL7Rα$^-$/c-Kit$^+$/Sca-1$^+$; common myeloid progenitors (CMPs) as Lin$^-$/IL7Rα$^-$/c-Kit$^+$/Sca-1$^-$/FcγR^{low}/CD34$^+$; granulocyte/macrophage progenitors (GMPs) as Lin$^-$/IL7Rα$^-$/c-Kit$^+$/Sca-1$^-$/FcγR^{high}/CD34$^+$; megakaryocyte/erythrocyte progenitors (MEPs) as Lin$^-$/IL7Rα$^-$/c-Kit$^+$/Sca-1$^-$/FcγR^{low}/CD34$^-$; and common lymphoid progenitors (CLPs) as Lin$^-$/IL7Rα$^+$/c-Kit^{low}/Sca-1^{low}.

Table 1. Forward and reverse primers

	Primer
Kras total-F	5′-CAAGAGCGCCTTGACGATAC-3′
Kras total-R	5′-GTACTGGTCCCTCATTGCAC-3′
*Kras*4A-F	5′-GAGACCTCAGCAAAGACAAG-3′
*Kras*4A-R	5′-TTCACACAGCCAGGAGTCT-3′
*Kras*4B-F	5′-ACAAGACAGGGTGTTGAC-3′
*Kras*4B-R	5′-TAACTGTACACCTTGTCCTT-3′
β-*Actin*-F	5′-GACGGCCAGGTCATCACTATTG-3′
β-*Actin*-R	5′-AGGAAGGCTGGAAAAGAGCC-3′

Statistical Analysis. All values are expressed as mean ± SD. *P* values were calculated with the unpaired Student's *t* test or Kruskal–Wallis test where indicated using GraphPad Prism software (v8.40). A *P* value above 0.05 was considered not significant. All significant *P* values are shown.

Data Availability. The raw data from the whole-exome sequencing analyses reported in this article have been deposited in the National Center for Biotechnology Information Sequence Read Archive under accession no. PRJNA732059 (38). All other data are available in the main text and supporting information.

ACKNOWLEDGMENTS. We thank Marta San Roman, Raquel Villar, and Nuria Cabrera for excellent technical assistance; Mayte Lamparero and Isabel Blanco (Animal Facility) for mouse work; the Histopathology Unit for processing of mouse tissues; Lola Martínez (Flow Cytometry Unit) for her help with flow cytometry analyses; Diego Megías and Manuel Perez (Confocal Microscopy Unit) for assistance with confocal microscopy; and the Mouse Genome Editing Unit for support with the generation of the mouse strains described here. We also thank Ignacio Perez de Castro (Instituto de Salud Carlos III, Madrid, Spain) for sharing the EGFP-KRAS4B plasmid and Orlando Dominguez (Genomics Unit) and Pedro P. Lopez-Casas (Clinical Research Program) for their advice on exome sequencing. This work was supported by grants from the European Research Council (ERC-2015-AdG/695566, THERACAN), the Spanish Ministry of Science, Innovation and Universities (RTC-2017-6576-1), and the Autonomous Community of Madrid (B2017/BMD-3884 iLUNG-CM); a grant from the CRIS Cancer Foundation (to M.B.); and a grant from the Spanish Ministry of Science, Innovation and Universities (RTI2018-094664-B-I00, to M.B. and M.M.). M.B. is a recipient of an Endowed Chair from the AXA Research Fund. M.S. was supported by predoctoral contract "Severo Ochoa" (BES-2016-079096) from the Spanish Ministry of Science, Innovation and Universities. G.P. was a recipient of a "Young Ph.D." grant from the Government of the Community of Madrid. F.F.-G. was supported by a formación de profesorado universitario (FPU) fellowship from the Spanish Ministry of Science, Innovation and Universities.

1. A. E. Karnoub, R. A. Weinberg, Ras oncogenes: Split personalities. *Nat. Rev. Mol. Cell Biol.* **9**, 517–531 (2008).
2. I. A. Prior, P. D. Lewis, C. Mattos, A comprehensive survey of Ras mutations in cancer. *Cancer Res.* **72**, 2457–2467 (2012).
3. M. Malumbres, M. Barbacid, RAS oncogenes: The first 30 years. *Nat. Rev. Cancer* **3**, 459–465 (2003).
4. D. K. Simanshu, D. V. Nissley, F. McCormick, RAS proteins and their regulators in human disease. *Cell* **170**, 17–33 (2017).
5. E. Castellano, E. Santos, Functional specificity of Ras isoforms: So similar but so different. *Genes Cancer* **2**, 216–231 (2011).
6. I. A. Prior, J. F. Hancock, Ras trafficking, localization and compartmentalized signalling. *Semin. Cell Dev. Biol.* **23**, 145–153 (2012).
7. B. Alvarez-Moya, C. López-Alcalá, M. Drosten, O. Bachs, N. Agell, K-Ras4B phosphorylation at Ser181 is inhibited by calmodulin and modulates K-Ras activity and function. *Oncogene* **29**, 5911–5922 (2010).
8. B. Sperlich, S. Kapoor, H. Waldmann, R. Winter, K. Weise, Regulation of K-Ras4B membrane binding by calmodulin. *Biophys. J.* **111**, 113–122 (2016).
9. M. T. Wang *et al.*, K-Ras promotes tumorigenicity through suppression of non-canonical Wnt signaling. *Cell* **163**, 1237–1251 (2015).

10. F. D. Tsai *et al*., K-Ras4A splice variant is widely expressed in cancer and uses a hybrid membrane-targeting motif. *Proc. Natl. Acad. Sci. U.S.A.* **112**, 779–784 (2015).
11. K. Weise *et al*., Membrane-mediated induction and sorting of K-Ras microdomain signaling platforms. *J. Am. Chem. Soc.* **133**, 880–887 (2011).
12. H. Jing *et al*., SIRT2 and lysine fatty acylation regulate the transforming activity of K-Ras4a. *eLife* **6**, e32436 (2017).
13. C. R. Amendola *et al*., KRAS4A directly regulates hexokinase 1. *Nature* **576**, 482–486 (2019).
14. L. Johnson *et al*., K-ras is an essential gene in the mouse with partial functional overlap with N-ras. *Genes Dev.* **11**, 2468–2481 (1997).
15. K. Koera *et al*., K-ras is essential for the development of the mouse embryo. *Oncogene* **15**, 1151–1159 (1997).
16. S. J. Plowman *et al*., While K-ras is essential for mouse development, expression of the K-ras 4A splice variant is dispensable. *Mol. Cell. Biol.* **23**, 9245–9250 (2003).
17. A. U. Newlaczyl, J. M. Coulson, I. A. Prior, Quantification of spatiotemporal patterns of Ras isoform expression during development. *Sci. Rep.* **7**, 41297 (2017).
18. J. Omerovic, D. E. Hammond, M. J. Clague, I. A. Prior, Ras isoform abundance and signalling in human cancer cell lines. *Oncogene* **27**, 2754–2762 (2008).
19. S. J. Plowman *et al*., K-ras 4A and 4B are co-expressed widely in human tissues, and their ratio is altered in sporadic colorectal cancer. *J. Exp. Clin. Cancer Res.* **25**, 259–267 (2006).
20. C. E. Patek *et al*., Mutationally activated K-ras 4A and 4B both mediate lung carcinogenesis. *Exp. Cell Res.* **314**, 1105–1114 (2008).
21. M. D. To *et al*., Kras regulatory elements and exon 4A determine mutation specificity in lung cancer. *Nat. Genet.* **40**, 1240–1244 (2008).
22. R. Nussinov, C. J. Tsai, H. Jang, Oncogenic Ras isoforms signaling specificity at the membrane. *Cancer Res.* **78**, 593–602 (2018).
23. M. Drosten *et al*., Genetic analysis of Ras signalling pathways in cell proliferation, migration and survival. *EMBO J.* **29**, 1091–1104 (2010).
24. M. Sanclemente *et al*., c-RAF ablation induces regression of advanced Kras/Trp53 mutant lung adenocarcinomas by a mechanism independent of MAPK signaling. *Cancer Cell* **33**, 217–228.e4 (2018).
25. C. Guerra *et al*., Tumor induction by an endogenous K-ras oncogene is highly dependent on cellular context. *Cancer Cell* **4**, 111–120 (2003).
26. E. L. Jackson *et al*., The differential effects of mutant p53 alleles on advanced murine lung cancer. *Cancer Res.* **65**, 10280–10288 (2005).
27. W. C. Chen *et al*., Regulation of KRAS4A/4B splicing in cancer stem cells by the RBM39 splicing complex. *BioRxiv* [Preprint] (2019). https://dx.doi.org/10.1101/646125 (Accessed 1 November 2020).
28. N. Potenza *et al*., Replacement of K-Ras with H-Ras supports normal embryonic development despite inducing cardiovascular pathology in adult mice. *EMBO Rep.* **6**, 432–437 (2005).
29. M. Drosten *et al*., H-Ras and K-Ras oncoproteins induce different tumor spectra when driven by the same regulatory sequences. *Cancer Res.* **77**, 707–718 (2017).
30. T. Pantsar, The current understanding of KRAS protein structure and dynamics. *Comput. Struct. Biotechnol. J.* **18**, 189–198 (2019).
31. J. K. Voice, R. L. Klemke, A. Le, J. H. Jackson, Four human Ras homologs differ in their abilities to activate Raf-1, induce transformation, and stimulate cell motility. *J. Biol. Chem.* **274**, 17164–17170 (1999).
32. X. Zhang, J. Cao, S. P. Miller, H. Jing, H. Lin, Comparative nucleotide-dependent interactome analysis reveals shared and differential properties of KRas4a and KRas4b. *ACS Cent. Sci.* **4**, 71–80 (2018).
33. S. I. Chung *et al*., Comparison of liver oncogenic potential among human RAS isoforms. *Oncotarget* **7**, 7354–7366 (2016).
34. F. McCormick, K-Ras protein as a drug target. *J. Mol. Med. (Berl.)* **94**, 253–258 (2016).
35. J. Canon *et al*., The clinical KRAS(G12C) inhibitor AMG 510 drives anti-tumour immunity. *Nature* **575**, 217–223 (2019).
36. J. Hallin *et al*., The KRASG12C inhibitor, MRTX849, provides insight towards therapeutic susceptibility of KRAS mutant cancers in mouse models and patients. *Cancer Discov.* **10**, 54–71 (2020).
37. C. L. Lee *et al*., Generation of primary tumors with Flp recombinase in FRT-flanked p53 mice. *Dis. Model. Mech.* **5**, 397–402 (2012).
38. M. Salmón *et al*., Comparison of mutations in lung tumors driven by KRASG12V/Trp53-KO and KRAS4AG12V4B-/Trp53-KO. National Center for Biotechnology Information (NCBI) Sequence Read Archive. https://www.ncbi.nlm.nih.gov/sra/PRJNA732059. Deposited 22 May 2021.